PCCP

COMMUNICATION

View Article Online
View Journal | View Issue

Fe–N bonding in a carbon nanotube–graphene complex for oxygen reduction: an XAS study†

Cite this: *Phys. Chem. Chem. Phys.*, 2014, **16**, 15787

Received 3rd April 2014,
Accepted 12th June 2014

DOI: 10.1039/c4cp01455c

www.rsc.org/pccp

Jigang Zhou,*[ab] Paul N. Duchesne,[c] Yongfeng Hu,[a] Jian Wang,[a] Peng Zhang,[c] Yanguang Li,[d] Tom Regier[a] and Hongjie Dai[d]

The electronic structure study of carbon nanotube–graphene complexes has been performed using comprehensive X-ray absorption spectroscopy (XAS) at Fe L- and K-edges, along with C, N and O K-edges. The results obtained from the study of an iron-containing carbon nanotube–graphene complex (NT–G) have been compared in great detail with those of an iron-free carbon nanotube–graphene complex (pNT–G) and iron phthalocyanine (FePc). It has been confirmed that complex-like Fe^{3+} in a high spin state is the major iron component in NT–G. The C and N K-edge XANES further confirmed that Fe is very likely to be bonded to N in NT–G. This Fe–N species should be the active site for enhanced oxygen reduction reaction (ORR) activity in NT–G. A unique O K-edge X-ray absorption spectroscopic feature has been observed in NT–G, which might be caused by chemisorbed O_2 on the Fe–N site. Such knowledge is important for the understanding of this specific complex, and the knowledge should benefit the rational design of other carbon/metal/nitrogen-containing ORR catalysts with further improved performance.

The rational design of novel catalysts to boost the slow oxygen reduction reaction (ORR) process in acidic environments, especially as cost-effective alternatives to precious metal-based ones, has evolved into an intense search to facilitate the widespread application of proton-exchange membrane fuel cells.[1–3] Unfortunately, this search has met with limited success, due to a poor understanding of the intrinsic relationship between the catalyst's ORR active sites and catalytic performance. Alongside ongoing efforts to optimize transition metal/nitrogen-containing, carbon-based ORR catalysts,[4,5] a new class of ORR catalysts with high catalytic activity and stability has been developed by selectively unzipping the outer wall of few-walled carbon nanotubes (CNTs), followed by annealing in NH_3 to make a graphene–CNT complex. Trace iron originating from the Fe catalyst (used to seed CNT growth) is essential for making NT–G a highly efficient ORR catalyst.[1] Leaching out iron before unzipping CNTs yielded a similar nanotube–graphene complex (so-called "purified NT–G" or pNT–G) with some ORR activity.[1] Raman and TEM analyses indicated that pNT–G is almost identical to NT–G in terms of the carbon frame matrix, and N 1s XPS confirmed their similar N environments. The only difference between NT–G and pNT–G is iron content (0.24 at% in NT–G *vs.* 0.03 at% in pNT–G) and this difference caused a huge ORR activity difference (a significant loss in ORR activity with the half-wave potential moving in the negative direction for ~100 mV in pNT–G). Furthermore, electron energy loss spectroscopy (EELS) mapping of Fe and N atoms revealed their proximity on the graphene sheets and suggested that Fe–N in NT–G might be the ORR active sites, similar to metal–nitrogen catalysts.[1] This assumption is further supported by the suppression of ORR activity in the presence of cyanide (it is known that Fe-based ORR catalysts can be poisoned *via* adsorption of CN^-).[1] These findings opened a new avenue for highly efficient, low-cost and durable ORR catalysts in acidic media and, for the first time, experimentally confirmed the space proximity of Fe and N atoms in such ORR catalysts. However a deeper and more fundamental understanding of the structure of NT–G is still needed to provide more insights into its detailed chemical and electronic structures (for instance, how Fe is bonded to N and what are the valence and spin states of Fe), which are directly relevant to ORR activity. Such studies shall serve as a foundation for further investigation of even better catalysts. In addition to its practical application, a fundamental spectroscopic study of this new complex (a combination of graphene sheets and CNTs) is also attractive. X-ray absorption spectroscopy, consisting of the near edge structure (XANES) and extended edge structure (EXAFS), involves the measurement and interpretation of the photoabsorption cross-section, across a particular core level (absorption edge) of an atom in a chemical environment, up to ~50 eV above the threshold in XANES and ~1000 eV above the

[a] *Canadian Light Source Inc, Saskatoon, Canada.*
E-mail: jigang.zhou@lightsource.ca; Fax: +1-306-6573535; Tel: +1-306-657-3587
[b] *School of Chemical Engineering, Harbin Institute of Technology, China*
[c] *Department of Chemistry, Dalhousie University, Halifax, Canada*
[d] *Department of Chemistry, Stanford University, Stanford, USA*

† Electronic supplementary information (ESI) available: C K-edge XANES spectra of NT-G, pNT-G, CNTs and oxidized CNTs. O K-edge XANES spectra of NT-G, pNT-G, CNTs and oxidized CNTs before edge normalization. See DOI: 10.1039/c4cp01455c

edge in EXAFS. The absorption features in XANES track bound-to-bound and bound-to-quasi-bound electronic transitions and multiple scattering. This technique is element specific and very sensitive to the local chemical environment of the absorbing atom. Whereas XANES is powerful in revealing the structure and bonding in nanomaterials, particularly carbon nanostructure hybrids,[6–8] EXAFS is sensitive to geometric factors such as bond lengths and coordination environments.

This article reports an application of Fe L- and K-edge XANES, and Fe K-edge EXAFS, as well as C, N, and O K-edge XANES to study the chemical structure of NT–G in comparison to that of pNT–G, CNTs, and iron phthalocyanine (FePc). The goal is to spectroscopically investigate the Fe–N based ORR activity center in NT–G, which can only be achieved through a comprehensive soft and hard X-ray spectroscopic study probing the different elements and absorption edges in this complex system. NT–G and pNT–G were prepared by first oxidizing few-walled CNTs (to yield oxidized CNTs) *via* a modified Hummers' method, followed by annealing the oxidized product in NH_3. The preparation details can be found in a previous publication.[1] Briefly, CNTs grown from iron seeds were initially oxidized using concentrated H_2SO_4 for 24 hours and then further oxidized *via* the addition of $KMnO_4$ to this solution for 2 hours before the oxidation was quenched with ice and H_2O_2 solution. At this stage, oxidized NT–G was collected *via* centrifugation and annealed under an atmosphere of 2 torr 10% NH_3/Ar at high temperature to afford nitrogen doping and restoration of sp^2 carbon centres to produce NT–G. The control sample, pNT–G, was made by leaching out the trace iron seed in the CNT sample using concentrated HCl before implementing the same oxidation and N-doping procedure used in making NT–G. The XAS measurement of powder samples was performed at the SGM beamline in a vacuum chamber at $\sim 10^{-8}$ torr, and data were recorded using the surface-sensitive total electron yield (TEY) method with a probing depth of 1–10 nm.[11] Fe K-edge XAS was performed at the SXRMB beamline and data were recorded using both TEY and fluorescence yield (FY). Only FY EXAFS data were presented, as the TEY EXAFS data were significantly noisier due to low Fe concentrations in the samples. TEY XANES was used to confirm that Fe K-edge FY spectra were not saturated due to the sample self-absorption. Signal intensity was first normalized to the incident photon flux (I_0) upstream of the sample, measured using a fresh gold mesh at SGM and an ion chamber at SXRMB. After background correction, the XANES spectra were normalized to the edge jump (the difference in the absorption coefficient just below and at a flat region above the edge). Experimental EXAFS plots were obtained using WinXAS software[9] by applying a Fourier Transform to the data between 2.5 and 12.5 $Å^{-1}$ for each absorption spectrum. Fitting was performed within a specific region of interest for each sample (FePc: 1.0–3.0 Å, CNT: 1.3–2.6 Å, and NT–G: 1.4–2.55 Å). Uncertainties were determined by weighting the off-diagonal elements of the correlation matrix by the reduced χ^2 value of the fit, as recommended by Newville *et al.*[10] Details specific to the fitting of each sample are presented in the ESI.†

The electronic structure of the Fe site in NT–G was first studied using Fe L-edge XANES, as shown in Fig. 1a. The L-edge

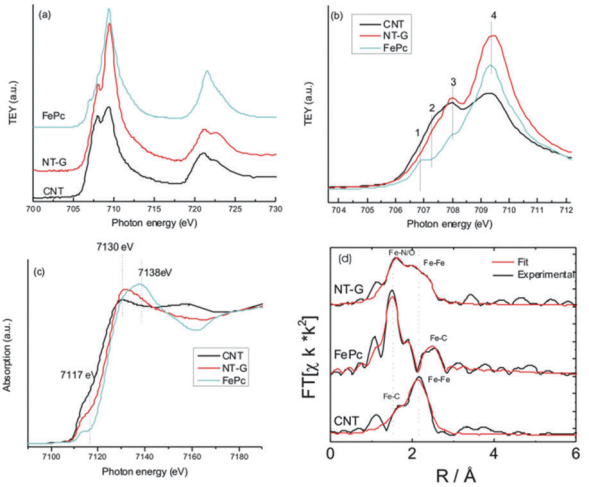

Fig. 1 Fe L-edge XANES spectra of NT–G, FePc, and CNTs (a), enlarged L_3 edge spectra in Fe L-edge XANES (b), Fe K-edge XANES spectra (recorded FY mode) of NT–G, FePc, and CNTs (c), and FT EXAFS spectra of NT–G, FePc, and CNTs (d).

of 3d transition metals results from electronic transitions between the 2p level and the largely unoccupied 3d electronic states. The spectral features at this edge are sensitive to the valence and spin states of the probed atom.[11,12] The spin–orbit splitting of the Fe 2p orbitals causes two groups of peaks in the Fe L-edge spectrum (*i.e.* the L_3 edge and L_2 edge, ranging from 706 eV to 712 eV and from 718 eV to 726 eV, respectively). The former involves transitions from Fe $2p_{3/2}$ to Fe 3d states, while the latter comes from transition from Fe $2p_{1/2}$ to Fe 3d states. Both L_3- and L_2-edge features are further split by the ligand field due to final state effects, especially at the L_3-edge. Here in Fig. 1a, the Fe L-edge of NT–G is compared to those of iron phthalocyanine (FePc) and CNTs; from the overall spectral shape we can conclude that there are structural differences between them. Detailed structural differences can be more easily found by focusing on the L_3-edge region shown in Fig. 1b. First of all, the mean oxidation state of Fe in NT–G will be lower than that in FePc and higher than that in CNTs, as evidenced by the absorption edge position. Secondly, NT–G exhibits peaks similar to both FePc (peak 1 at ~706.9 eV) and CNTs (peak 2 at ~707.5 eV), but these are not as well resolved as those of CNTs and FePc. Peak 2 may be attributed to metallic Fe,[13] a reasonable observation due to the existence of metallic Fe in the iron seed catalyst used to grow the CNTs.[1] This metallic iron may interact with the CNTs *via* Fe–C bonding, giving rise to the spectroscopic feature at peaks 3 (~708 eV) and 4 (~709.5 eV) in CNTs.[13] The lower intensity and breadth of peak 2 in NT–G indicate the presence of less metallic iron in NT–G, relative to CNTs. Finally, the ratios of peak 4 to peak 3 in both NT–G and FePc indicate Fe^{3+} in a high spin state.[12] It is reasonable to compare the Fe spectrum of NT–G to that of FePc (a macrocyclic organometallic complex with a central Fe atom coordinated by four pyrrolic N functional groups, which exhibits ORR activity[12]) since the possibility of Fe–N bonding is supported by the proximity of Fe and N atoms determined *via* EELS mapping

in our previous study.[1] It has been established that the iron in pristine FePc is Fe^{2+} in an intermediate-spin state, and that this Fe^{2+} will be converted to an Fe^{3+}-like high spin form after exposure to oxygen.[11,12] Both NT–G and FePc in this study were greatly exposed to air, and therefore we expect to see a high spin Fe^{3+} in both samples. The Fe L-edge spectrum of FePc reported here is actually very similar to the reported spectra of oxygen-exposed FePc in Fig. 1 of ref. 11 and Fig. 4 of ref. 12 as summarized in Table S1 in the ESI.† It should be noted that even though FePc is a good reference compound to explore the possible Fe–N bonding in NT–G, NT–G has a much more complicated structure (trace iron dispersed in a CNT–graphene complex) and much better ORR activity than FePc. These differences in structure and performance are reflected by the spectral differences observed in Fig. 1a and b between FePc and NT–G. Further calculation of XAS-related properties such as charge-transfer[12] shall be useful to obtain a deeper understanding of the experiment. The Fe–N bonding in our NT–G will be further confirmed using N K-edge XANES in the following sections, and possible O_2 chemisorption on NT–G (especially at Fe) will be further evaluated using O K-edge XANES. But let's focus on the Fe chemical environment by comparing the Fe K-edge XANES and EXAFS of NT–G with those of FePc and CNTs, as displayed in Fig. 1c and d. Fe K-edge XANES involves a 1s to 4p dipole transition and is also sensitive to the oxidation state and bonding geometry.[2] The absorption edge position shifts to higher energy in NT–G relative to CNTs but it is lower than that of FePc, again confirming an oxidation state of Fe in NT–G that is intermediate between those of CNTs and FePc, as was observed for Fe L-edge XANES. The Fe K-edge XANES feature at 7130 eV and the pre-edge feature at ~7117 eV in NT–G could be due to Fe with a planar local symmetry, which have been observed for iron(II) phthalocyanine (Fe^{2+}Pc).[2] A lower-intensity pre-edge feature at 7113 eV and an additional main absorption peak at ~7140 eV in FePc here can correspond to Fe^{3+}Pc due to a more strong oxygen adsorption on FePc.[2] Fe K-edge EXAFS spectra in Fig. 1d further show the Fe bonding environment in NT–G; the corresponding parameters are shown in Table S2 in the ESI.† Based on the compositions of these samples, and in conjunction with the XANES results discussed previously, scattering paths of Fe–C and Fe–N/O were assigned to CNTs and NT–G, respectively. Metallic Fe–Fe bonding is observed in both samples, with very similar coordination numbers and bond distances. In contrast, the Fe–N/O coordination number in NT–G is more than twice that of Fe–C in CNTs, indicating a significantly greater degree of Fe–N and Fe–O bonding; this could help explain the increased catalytic activity of NT–G, as these Fe–N/O environments are believed to be responsible for the catalytic activity of FePc and other similar compounds. Fe–N bonding can be fitted in FePc with a bond length close to that of NT–G, which again supports Fe–N bonding in NT–G. A third scattering path, attributed to Fe–O bonding, was also observed between the expected Fe–N/O and Fe–C paths. It can be understood that NT–G and FePc are merely similar and not identical, as was also observed in Fe L-edge XANES. Considering the enrichment of Fe and N along the edge of graphene sheets, it is logical for NT–G to have a lower Fe–N/O coordination number (3.3–3.6) than that in FePc (Fe–N = 4 and Fe–O = 2).

In Fig. 2a, we further examine the nitrogen chemical environment in NT–G and pNT–G using N K-edge XANES in order to better understand the Fe–N bonding in NT–G. N K-edge XANES probes N 2p electronic states; the sharp peaks at ~398 eV (peak a) and ~401.5 eV (peak c) can be assigned to π* transition to pyridinic and pyrrolic states, respectively, and the peak at ~408 eV is due to C–N σ* transitions.[14] In addition to the pyridinic and pyrrolic bonding in NT–G and pNT–G, a new feature at ~399 eV (indicated by an arrow in Fig. 2a, inset) is resolved in NT–G which is definitely absent in the spectrum of pNT–G. This feature could be due to the Fe–N bonding as suggested by XPS in Fe–N–C structure,[2] and is also in agreement with the above Fe L- and K-edge study. Such Fe–N bonding should weaken the C–N bond and will cause the C–N σ* feature to shift to lower energy[15] as is the case in NT–G. It is reasonable to exhibit only a very small Fe–N bonding relative to N–C (pyridine and pyrrolic) in NT–G because of the lower iron content relative to N (0.24 at% Fe *vs.* 5 at% N) and only some of this iron can be bonded to N. C K-edge XANES spectra of NT–G, pNT–G and CNT are displayed in Fig. 2b and used to study the chemistry and electronic structure of these samples to find out if the Fe–N bonding in NT–G changes the carbon matrix structure. C K-edge XANES is dominated by the transition from C 1s electrons to mainly C 2p states, following the dipole selection rules. It is dominated by two main transitions at ~285 eV (peak b) and ~292 eV (peak d) attributable to C 1s transitions to the graphitic C–C π* and C–C σ* states, respectively. The existence of these π* transition peaks in all samples confirms the existence of their graphitic networks. The relatively low intensity of π* and σ* peaks of NT–G and pNT–G relative to that of CNTs should be due to the damage to the sp^2 carbon crystallinity either from unzipping of the outer wall of the CNTs or the N doping. The sp^2 carbon disruption is also indicated by the broadened σ* peaks in NT–G and pNT–G relative to the well-resolved double σ* peaks in CNTs, since the excitonic state peak at ~292 eV comes from a well-crystallined sp^2 carbon network.[16] The absorption band at ~288 eV (peak c) in NT–G and pNT–G must be due to residual oxygen functional groups, since this feature is visible in the same position as that in oxidized CNTs (Fig. S1, ESI†). The carbon environment, including C–C and C–O bonding, in NT–G is identical to that in pNT–G. Considering the emergence of a subtle new N feature and the identical C environment in NT–G

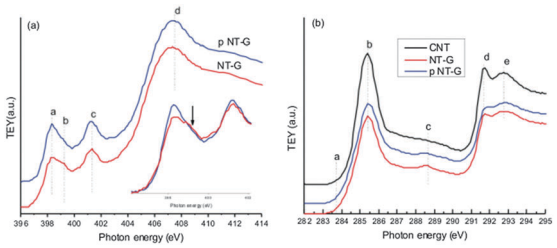

Fig. 2 XANES spectra of NT–G, pNT–G and CNTs at the N K-edge and enlarged π* transition (inset) (a), and C K-edge (b) recorded in TEY mode.

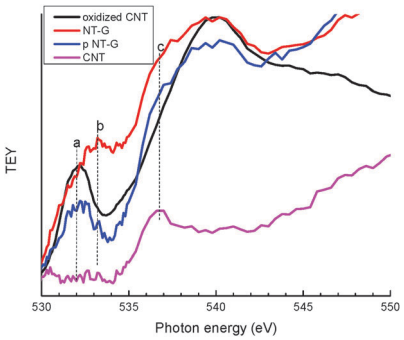

Fig. 3 O K-edge XANES spectra of NT–G, pNT–G and Pt black.

relative to that of pNT–G, we are more confident with the assignment of Fe–N bonding in NT–G, and that this Fe–N bonding shall be responsible for the enhanced ORR activity in NT–G.

Finally, O K-edge XANES spectra of NT–G, together with NT–G, CNT and oxidized CNT are shown in Fig. 3. In Fig. S2 (ESI†), non-normalized O K-edge spectra clearly show a much lower oxygen concentration for annealed samples (NT–G and pNT–G) relative to the oxidized CNTs, which is reasonable since annealing reduces C–O bonds in oxidized CNTs to restore sp^2 carbon.[1] To highlight the chemical differences between these samples, the O K-edge XANES spectra have been normalized to unity at the edge jump. O K-edge spectra probe the unoccupied O 2p projected states, which could be hybridized with metal d orbitals in metal oxides[6] or carbon p orbitals. Both pNT–G and NT–G have a peak at ~532 eV (peak a) which can be assigned to the residual C–O bond from an incomplete sp^2 restoration of oxidized C after its annealing in NH_3. This peak aligns with the spectral feature of oxidized CNTs, the surface of which is rich in oxygen functional groups, but it is absent for pristine CNTs. This C–O bonding has an associated σ* bonding feature at ~540 eV. In addition to those features, NT–G and pNT–G also have a shoulder peak at ~537 eV (peak c) which aligns with the oxygen peak in CNTs. Considering that there is only very weak C–O bonding in CNTs, as suggested by the C K-edge XANES in Fig. 2, it should be reasonable to assign this feature in CNTs to chemisorbed O_2 which shall occur at a lower energy relative to the molecular oxygen (the σ* of free O_2 lies at an energy higher than 540 eV, ref. 17). This shift to lower energy in chemisorbed O_2 is due to electron gain by oxygen from CNTs[18] to form O_2^--like species. Therefore, the shoulder peak at NT–G and pNT–G at ~537 eV shall be due to the chemisorbed O_2, as was observed in CNTs. Very interestingly, in addition to all those common features, NT–G also presents a unique feature shown at ~533 (peak b) eV. Using O K-edge XANES, catalytically active oxygen (chemisorbed O_2) has been observed to show peaks at ~533 eV in $LaSrCoO_3$ (a good oxygen electrode material).[19] In addition, O_2^- species have been observed at the same energy position in LiO_2 in a discharged Li-air cathode.[20] Therefore, it is possible that this new oxygen feature in NT–G can be linked to a chemisorbed O_2 and may be in the form of O_2^-. The σ* feature in the O K-edge XANES spectra of chemisorbed O_2 can be used to estimate the O–O bond length,[17] in which a shorter bond corresponds to a higher energy shift. Considering the similarity of the oxygen functional groups (from C K-edge XANES) and C–N bonding (from N K-edge XANES) environments in NT–G and pNT–G, this chemisorbed O_2 in NT–G can only be associated with the Fe–N site.

In summary, the detailed electronic and chemical structures in a novel graphene–CNT complex (NT–G) have been studied using comprehensive XAS involving multiple elements and absorption edges. The Fe XANES and EXAFS show that the most likely Fe bonding in NT–G is Fe–N, which holds a high spin Fe^{3+} state possibly due to O_2 chemisorption. The emergence of a subtle, new N feature in N K-edge XANES strengthens the Fe–N assignment. Such Fe–N bonding and its electronic structure modification upon oxygen adsorption could benefit from advanced DFT calculations for those samples with extremely low Fe concentration (0.24 at% Fe) and its random distribution in a distorted CNT–graphene complex.

We thank Dr J. Dynes and Q. Xiao and X. Chen at CLS for technical assistance and Professor Frank M. F. de Groot at Utrecht University in The Netherland for discussion. CLS is supported by NSERC, NRC, CIHR and the University of Saskatchewan.

Notes and references

1 Y. Li, W. Zhou, H. Wang, L. Xie, Y. Liang, F. Wei, J.-C. Idrobo, S. J. Pennycook and H. Dai, *Nat. Nanotechnol.*, 2012, **7**, 394–400.
2 M. Ferrandon, A. J. Kropf, D. J. Myers, K. Artyushkova, U. Kramm, P. Bogdanoff, G. Wu, C. M. Johnston and P. Zelenay, *J. Phys. Chem. C*, 2012, **116**, 16001–16013.
3 H. A. Gasteiger, S. S. Kocha, B. Sompalli and F. T. Wagner, *Appl. Catal., B*, 2005, **56**, 9–35.
4 G. Wu, K. L. More, C. M. Johnston and P. Zelenay, *Science*, 2011, **332**, 443–447.
5 M. Lefevre, E. Proietti, F. Jaouen and J. P. Dodelet, *Science*, 2009, **324**, 71–74.
6 J. G. Zhou, H. T. Fang, Y. F. Hu, T. K. Sham, C. X. Wu, M. Liu and F. Li, *J. Phys. Chem. C*, 2009, **113**, 10747–10750.
7 J. G. Zhou, H. T. Fang, J. M. Maley, J. Y. P. Ko, M. Murphy, Y. Chu, R. Sammynaiken and T. K. Sham, *J. Phys. Chem. C*, 2009, **113**, 6114–6117.
8 S. Yang, D. Wang, G. Liang, Y. M. Yiu, J. Wang, L. Liu, X. Sun and T.-K. Sham, *Energy Environ. Sci.*, 2012, **5**, 7007–7016.
9 T. Ressler, *J. Synchrotron Radiat.*, 1998, **5**, 118–122.
10 M. Newville, B. I. Boyanov and D. E. Sayers, *J. Synchrotron Radiat.*, 1999, **6**, 264–265.
11 P. L. Cook, X. S. Liu, W. L. Yang and F. J. Himpsel, *J. Chem. Phys.*, 2009, **131**, 194701.
12 P. S. Miedema, M. M. van Schooneveld, R. Bogerd, T. C. R. Rocha, M. Hävecker, A. Knop-Gericke and F. M. F. de Groot, *J. Phys. Chem. C*, 2011, **115**, 25422–25428.
13 C. L. Yueh, J. C. Jan, J. W. Chiou, W. F. Pong, M.-H. Tsai, Y. K. Chang, Y. Y. Chen, Y. F. Lee, P. K. Tseng, S. L. Wei, C. Y. Wen, L. C. Chen and K. H. Chen, *Appl. Phys. Lett.*, 2001, **79**, 3179–3181.

14 J. Wang, J. Zhou, Y. F. Hu and T. Regier, *Energy Environ. Sci.*, 2013, **6**, 926–934.
15 J. G. Zhou, X. T. Zhou, R. Y. Li, X. L. Sun, Z. F. Ding, J. Cutler and T. K. Sham, *Chem. Phys. Lett.*, 2009, **474**, 320–324.
16 J. G. Zhou, J. Wang, H. T. Fang, C. X. Wu, J. N. Cutler and T. K. Sham, *Chem. Commun.*, 2010, **46**, 2778–2780.
17 J. Stohr, *NEXAFS Spectroscopy*, Springer, Berlin, 1996.
18 P. G. Collins, K. Bradley, M. Ishigami and A. Zettl, *Science*, 2000, **287**, 1801–1804.
19 M. Imamura, N. Matsubayashi and H. Shimada, *J. Phys. Chem. B*, 2000, **104**, 7348–7353.
20 B. M. Gallant, D. G. Kwabi, R. R. Mitchell, J. Zhou, C. V. Thompson and Y. Shao-Horn, *Energy Environ. Sci.*, 2013, **6**, 2518–2528.